Asian Journal of Chemistry; Vol. 34, No. 6 (2022), 1493-1497

ASIAN JOURNAL OF CHEMISTRY

https://doi.org/10.14233/ajchem.2022.23723

A Comparative Study of Structural, Morphological and Optical Properties of Pure and Tellurium-Doped ZnO Nanostructures

ANIL U. SONAWANE* and B.K. SONAWANE

Department of Electronics, J.D.M.V.P. Co-Operative Samaj's Arts, Commerce and Science College, Jalgaon-425301, India

*Corresponding author: E-mail: bksonawane9963@gmail.com

Received: 11 January 2022; *Accepted*: 2 March 2022; *Published online*: 18 May 2022; AJC-20812

Pure and tellurium-doped ZnO nanostructure films were prepared on microscopic glass substrates using the sol-gel method and investigated the relationship between the structural, morphological, roughness, and optical properties. The X-ray diffraction (XRD) spectra revealed that the nanostructure films have a hexagonal Wurtzite structure. The field emission scanning electron microscope (FESEM) images showed that the surface morphology of the nanostructure films was modified due to the Te dopant. The atomic force microscopy (AFM) technique was used to study the surface roughness of the pure ZnO and Te-doped ZnO deposited films. The optical properties of the nanostructure films were obtained using the ultraviolet-visible spectrophotometer. The effects of Te dopant elements on the optical characteristics and the samples' energy band gaps were calculated and discussed.

Keywords: Tellurium, ZnO, Sol-gel, Nanostructure, Bond length, AFM.

INTRODUCTION

In many optoelectronic applications, such as lasers, solar cells, light-emitting devices and detectors, wide bandgap semiconductors have been considered as the most energetic materials [1]. Zinc oxide (ZnO) is one of the mostly stable, Wurtzite hexagonal type structures, with wide direct band gaps, II-VI compound semiconductor materials. At room temperature, ZnO has a wide optical bandgap at around 3.3 eV, absorbs light in the UV range, and has a high exciton binding energy (60 meV) [2,3]. Pure ZnO nanostructured films have some limitations; pure ZnO films showing n-type conductivity, optical and electrical properties are unstable. Therefore, ZnO can not be used in pure form, thus requires doping with other appropriate materials [4,5]. Also, to develop various additional characteristics of pure ZnO, it is essential to tailor its optical, structure, and morphological properties according to the scope of new devices.

Modified ZnO nanostructures have been recently doped with chalcogen elements such as S, Se and Te [6,7]. Among these elements, tellurium is a suitable ionic dopant for increasing the bandgap of ZnO. Tellurium has the most useful and interesting characteristics, such as higher infrared transparency, non-linear optical responses and photoconductivity, all of which have potential uses in optical and electronic devices [8,9]. Undoped ZnO and Te doped ZnO nanostructures films have been prepared using various deposition methods like chemical precipitation [10], spray pyrolysis [11], pulsed laser deposition [12], hydrothermal [13], sol-gel [14], *etc*. Among these techniques, sol-gel is particularly useful due of its cheap cost, lower processing temperature, environmental friendliness, and it requires no expensive equipment [15]. The main aim of the present work is to study the pure and Te-doped ZnO nanostructure films were prepared using the sol-gel method. A study of the films was carried out to examine the modifications in ZnO structural, surface and optical properties with the doping of tellurium.

EXPERIMENTAL

Pure ZnO and 10% Te doped ZnO nanostructure films were synthesized using the sol-gel spin coating method on the microscopic glass substrates. The starting precursors used for this deposition method were zinc acetate dihydrate, tellurium tetrachloride, 2-methoxyethanol and ethanolamine. For 0.4 M solution of pure ZnO was prepared using zinc acetate dihydrate

in 25 mL in 2-methoxy ethanol. The solution was stirred on a magnetic hot plate at ~75 ºC for 35 min. Ethanolamine (5 mL) was added to this solution as a reacting agent. The stirred was continued on a magnetic hot plate at the ~85 ºC for 30 min; the solutions became transparent and lastly aged for 6 h at room temperature. The prepared transparent solution was used for deposition on the pure ZnO nanostructure glass films. Previous to coating, microscopic glass substrates were cleaned with ethanol in an ultrasonic bath, distilled water and acetone.

The pure ZnO nanostructure films were deposited to the microscopic glass substrate using a spin coater system. The spin coater speed was maintained at 3000 rpm for 20 s. The deposition procedure was repeated ten times to complete the desired nanostructure film thickness. After each coating, all the nanostructure films were preheated at 200 ºC for 8 min. Finally, samples were post-annealed at 375 ºC for 1 h on the hot plate. Another 0.4 M solution of $TeCl_4$ was prepared in 25 mL in 2-methoxy ethanol for Te doped ZnO nanostructured films. Both solutions were mixed with a 10% ratio of tellurium solution. The final solution was treated in the same way as the pure ZnO nanostructure.

Characterization: For structural, surface morphological, roughness and optical properties of the deposited nanostructure film of pure ZnO and tellurium doping ZnO were carried out. An X-ray diffractometer (model: Rigaku Miniflex 600) with Cu*K*α radiation (λ = 1.54059Å) was used to examine the phase structure and the crystalline orientation of the films. A FESEM (Carl Zeiss Sigma) was used to study the surface morphology of deposited films. The atomic force microscopy (AFM) (TriA SPM) was used to observe the surface roughness of nanostructure film. A UV-visible spectrophotometer (model: Shimadzu UV-2600) was used to study optical properties.

RESULTS AND DISCUSSION

XRD studies: The XRD pattern of pure ZnO and 10% Te doped ZnO nanostructure glass films deposited using the sol-gel method are shown in Fig. 1. The XRD pattern observed that the pure ZnO nanostructure films have hexagonal wurtzite phase structures with corresponding JCPDS card no. 36-1451 [16], representing the film's strongly oriented *c*-axis. Inside the 10% Te doped ZnO films, additional impurity peaks identical to Te elements were observed at 2θ = 23.04º, 27.53º with JCPDS card no. 36-1452 [17]. This means the crystal structure has changed with the doping of Te into ZnO nanostructure. As

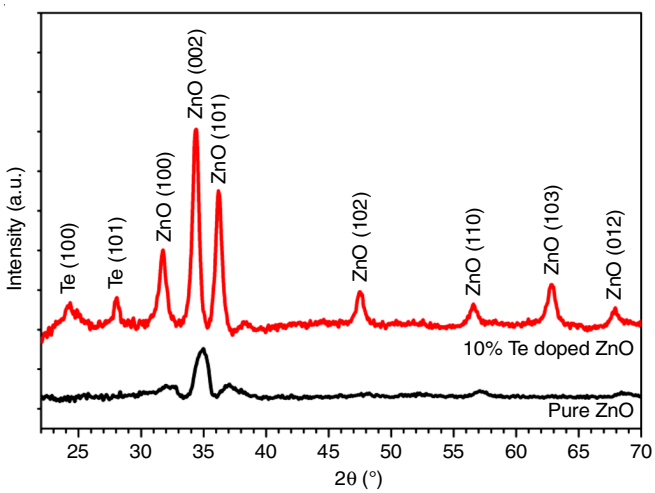

Fig. 1. XRD pattern for the pure ZnO and 10% Te doped ZnO nanostructure samples deposited using the sol-gel method

a consequence, it demonstrates that the nanostructure films have a hexagonal structure and a polycrystalline nature. The Te doping of ZnO film leads to sharper and stronger XRD peaks, an indication of higher crystallization. Tellurium doping increases the size of the crystallites and improves film crystallization as compared to pure ZnO film. The crystalline structure of Te doped ZnO nanostructure film is highly dependent on doping. Both nanostructure films have high diffraction peak intensity (002). A lower angle diffraction peak shifted (002) of 10% Te doped ZnO film outperforms pure ZnO because dissimilar ionic radii of Te ions were incorporated in the pure ZnO lattice. The reason for the shift in (002) diffraction peak is because of variations in lattice spacing a and c, as shown in Table-1.

It is observed an increase in the lattice parameters a and c as a result of the interstitial incorporation of Te ions with significant lattice defects. Other factors are responsible for increasing the lattice, such as oxygen vacancies, zinc antisites, strain and dislocation density.

The following equation was used to determine the Zn-O bond lengths (L) for pure ZnO and 10% Te doped ZnO nanostructure films [18]:

$$L = \sqrt{\left(\frac{a^2}{3}\right) + c^2[0.5 - u]^2}, \quad u = \frac{(a^2)}{(3c^2)} + \frac{1}{4}$$

where u is the positional parameter.

TABLE-1
THE DETAILED CALCULATIONS OF PLANES, d, LATTICE PARAMETERS, LATTICE CONSTANT (c/a) AND BOND LENGTH

Doping concentration	Planes (hkl)	d calculated	a (Å)	c (Å)	(c/a)	ZnO bond length L (Å)
Pure ZnO	ZnO (100)	2.7963	2.9699	5.1443	1.7322	1.9514
	ZnO (002)	2.5723				
	ZnO (101)	2.4283				
	ZnO (102)	1.8854				
	ZnO (110)	1.7487				
10% Te doped ZnO	Te (100)	3.6539	3.0100	5.2142	1.7323	1.9766
	Te (101)	3.1776				
	ZnO (100)	2.8176				
	ZnO (002)	2.6072				
	ZnO (101)	2.4794				

The calculated bond length for the pure ZnO and 10% Te doped ZnO nanostructure films was 1.9514 and 1.9766 Å, respectively. It was detected that the increase in Te, the bond length also increased. This can be due to the separation of ZnO lattice. The average crystalline size (D) was determined using Scherrer's formula from the high diffraction peak (002) [19].

$$D = \frac{\lambda K}{\beta \cos\theta}$$

where λ is the incident X-ray wavelength (1.5405 Å), K = 0.94, β is the Bragg diffraction angle and is full width at half maximum (FWHM). The values of peak position and FWHM are given in Table-2. The estimated average grain sizes for the deposited undoped ZnO and 10% Te doped ZnO nanostructure samples were found to be 11.70 and 19.63 nm, respectively.

Surface morphology and AFM study: The surface morphologies of undoped ZnO and 10% Te doped ZnO nanostructure films are observed through FESEM images (Fig. 2). The

TABLE-2
THE PEAK POSITION AND FWHM VALUES OF THE PURE ZnO AND 10% Te DOPED ZnO

Te doping concentration	Peak position, 2θ (°)	FWHM, β (°)
Pure ZnO	34.60	0.742
10% Te	34.37	0.442

FESEM images revealed that the undoped ZnO and Te doped ZnO nanostructure films with different surface morpho-logies and nanostructure crystalline natures were observed. The surface morphology and shape of pure ZnO nanostructure particles change with a 10% Te doping concentration, as seen in these images.The practical grain size of pure ZnO and 10% Te doped ZnO nanostructure films calculated from the FESEM graph was about 37 and 21 nm [20,21].

The AFM technique was used to study the surface morphology and surface roughness of the pure ZnO and 10% Te doped ZnO deposited nanostructure films. Fig. 3 shows the

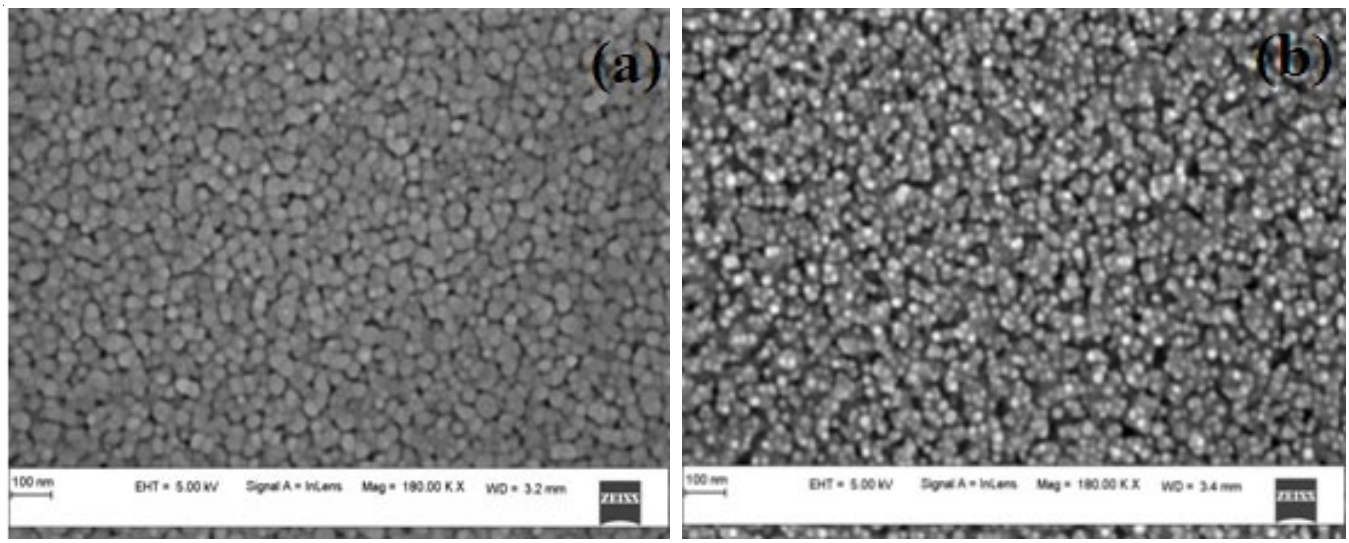

Fig. 2. FESEM image of (a) pure ZnO, (b) 10% Te doped ZnO nanostructure film

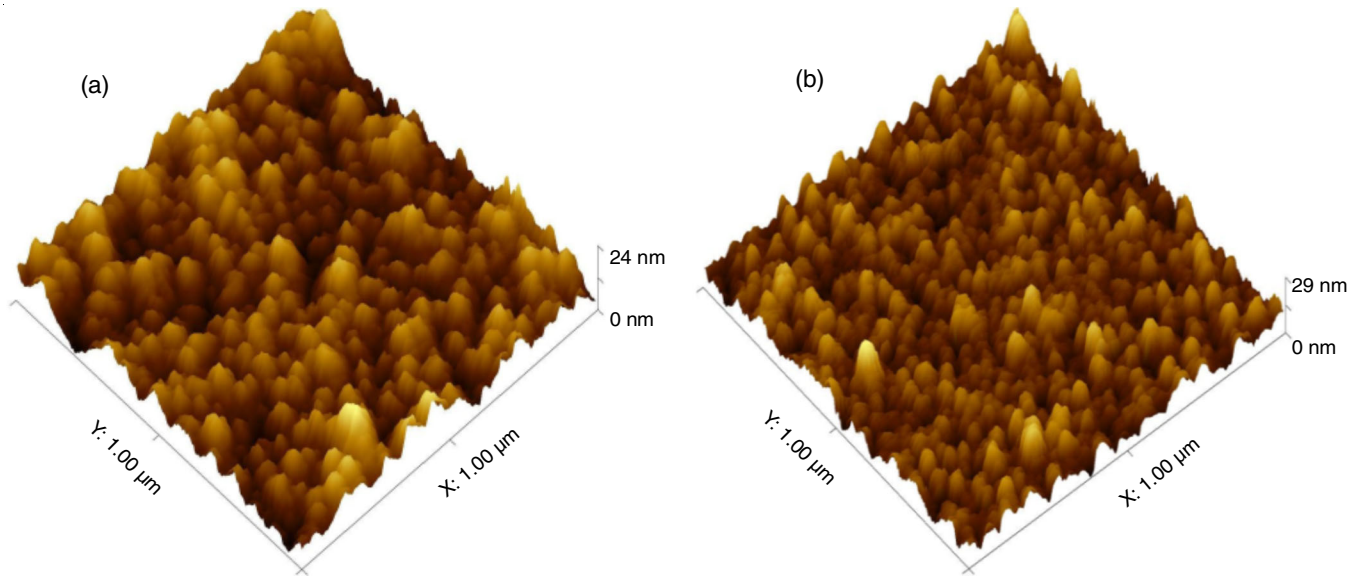

Fig. 3. (a) Pure, (b) Te doped ZnO nanostructure films of the surface roughness with 3D

AFM micrographs for pure ZnO and 10% Te doped ZnO nanostructure films of the surface roughness in 3D. It shows that pure films have a soft surface morphology, which increases with Te doping. AFM micrographs, the average surface roughness values of nanostructure films were found to be 9.94 and 10.99 nm, respectively for pure and 10% Te doped films. Also, the RMS roughness of pure ZnO and 10% Te-doped ZnO nanostructure films was estimated at 3.43 and 3.77 nm. An increase in the surface roughness was due to the more frequent clustering of nanosized granules due to the dispersion of ZnO with Te doping. The AFM results revealed that the average surface roughness value was increased by Te doped in ZnO [22,23].

Optical properties: The optical absorption and transmittance spectra for pure ZnO and 10% Te doped nanostructure films are shown in Fig. 4. Fig. 4a shows that both pure ZnO and 10% Te doped ZnO nanostructure films exhibited strong absorption edges across the UV wavelength region. The absorption edge was shifted to lower wavelengths from 364 to 355 nm as the Te doped nanostructure film. The intensity of the optical absorption edge of Te-doped ZnO nanostructure film increased gradually in the UV wavelength region with the increase in the concentration of tellurium. Te doped ZnO nanostructure films have the potential to improve UV light harvesting in optoelectronic devices [24,25].

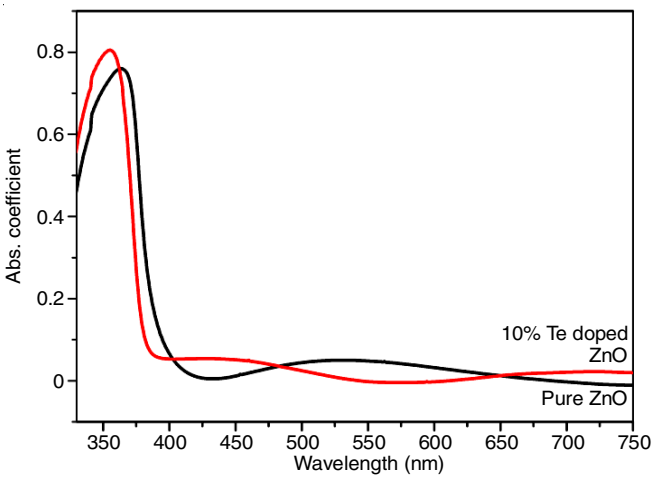

Fig. 4a. Absorption spectra for the pure and Te doped ZnO nanostructure films

Fig. 4b shows the optical transparency spectra from ultraviolet to near-infrared, which was determined to be ~88 % from 300 to 750 nm. The transmittance spectra of undoped ZnO and Te-doped ZnO nanostructure films were examined, and the average transparency decreased as Te doping concentration increased. Also, the transmittance edges were shifted to lower wavelengths when the percentage of Te increased [26,27].

The optical bandgap of pure and Te doped ZnO nanostructures films can be determined by Tauc's equation [28]:

$$(\alpha h\nu)^{1/n} = (h\nu - E_g)D^{1/n}$$

where hν the photon energy, α is the absorption coefficient and E_g is the optical bandgap and D is a constant. For a direct transition, the value of n =1/2 in this equation.

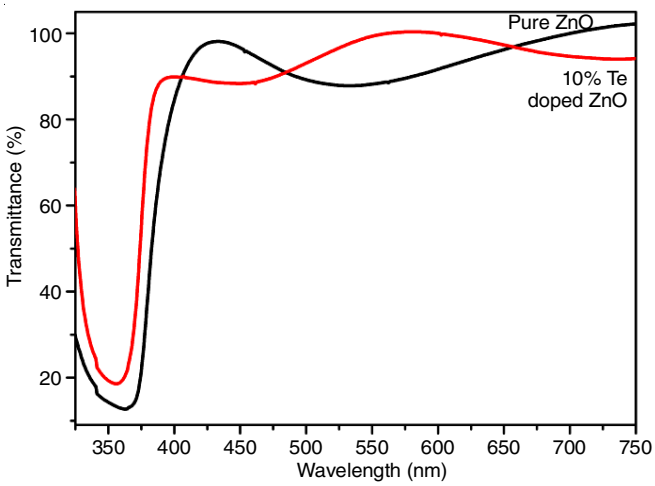

Fig. 4b. Optical transmittance spectra for the pure and Te doped ZnO nanostructure films

Fig. 5 shows the graph of $(\alpha h\nu)^2$ *vs.* photon energy (hν) of the deposited pure ZnO and 10% Te doped ZnO nanostructures films. For pure ZnO sample, the bandgap was calculated to be 3.214 eV. For the Te doped ZnO sample, the bandgap was observed to increase by increasing doping concentration and was similar to the results as reported earlier [29]. For 10% Te doped ZnO, the bandgap value was found to be 3.289 eV. The substantial change in the bandgap is due to tellurium doping in the ZnO nanostructure.

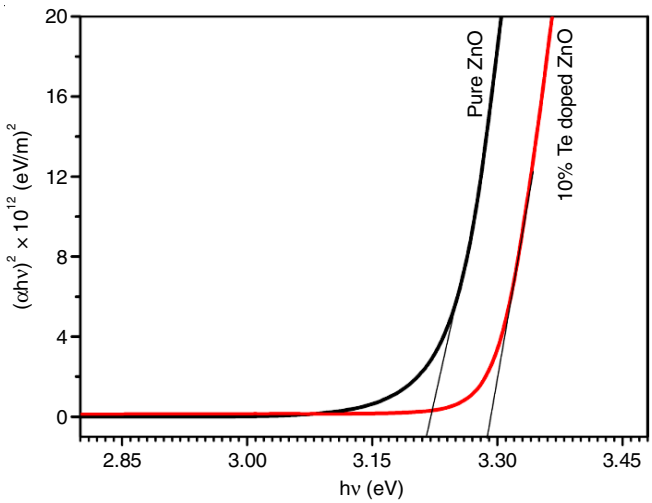

Fig. 5. Tauc's graph for the calculated of bandgap energy of pure ZnO and 10% Te doped ZnO nanostructures sample

Conclusion

Pure and 10% Te doped ZnO nanostructure films deposited using a sol-gel method on glass substrates was investigated and characterized by XRD, FESEM, AFM and UV-VIS methods. The XRD patterns showed both nanostructure films had hexagonal structures. The lattice parameters, bond length and crystalline size were increased in the 10% Te doped ZnO films. The surface morphology and shape of undoped ZnO sample particles were observed to change with Te doping concentration in FESEM images. The AFM micrographs observed the surface

roughness value increasing with Te doping ZnO films. The intensity of the optical absorption edge of the Te-doped ZnO nanostructure film was increased. The average transmittance of ~88% in the visible region for deposited films and transparency were decreased for increased Te doping concentration. The substantial variation in the bandgap is due to tellurium doping in the ZnO structure.

CONFLICT OF INTEREST

The authors declare that there is no conflict of interests regarding the publication of this article.

REFERENCES

1. L.J. Fitriani, A.D. Fitriani, B.R. Liasari, G.E. Timuda, W.B. Widayatno, A.S. Wismogroho, S. Zeng, M.D. Birowosuto and M.I. Amal, *Crystals*, **11**, 6 (2021); https://doi.org/10.3390/cryst11010006
2. E. Nowak, M. Szybowicz, A. Stachowiak, W. Koczorowski, D. Schulz, K. Paprocki, K. Fabisiak and S. Los, *J. Appl. Phys.*, **126**, 552 (2020); https://doi.org/10.1007/s00339-020-03711-2
3. B.K. Sonawane, M.P. Bhole and D.S. Patil, *Opt. Quantum Electron.*, **41**, 17 (2009); https://doi.org/10.1007/s11082-009-9317-y
4. M.A. Borysiewicz, *Crystals*, **9**, 505 (2019); https://doi.org/10.3390/cryst9100505
5. M.B. Agarwal, M. Malaidurai, A. Sharma and R. Thangavel, *Mater. Today*, **21**, 1781 (2020); https://doi.org/10.1016/j.matpr.2020.01.231
6. M. Sajjad, I. Ullah, M.I. Khan, J. Khan, M.Y. Khan and M.T. Qureshi, *Results Phys.*, **9**, 1301 (2018); https://doi.org/10.1016/j.rinp.2018.04.010
7. S. Mathew, P. Ganguly, V. Kumaravel, J. Harrison, S.J. Hinder, J. Barlett and S.C. Pillai, *Mater. Today*, **33**, 2458 (2020); https://doi.org/10.1016/j.matpr.2020.01.336
8. G. Tang, Q. Qian, X. Wen, G. Zhou, X. Chen, M. Sun, D. Chen and Z. Yang, *J. Alloys Comps.*, **633**, 1 (2015); https://doi.org/10.1016/j.jallcom.2015.02.007
9. F. Jamali-Sheini, R. Yousefi, M.R. Mahmoudian, N.A. Bakr, A. Saaedi and N.M. Huang, *Ceram. Int.*, **40**, 7737 (2014); https://doi.org/10.1016/j.ceramint.2013.12.115
10. C. Prabakar, S. Muthukumaran and V. Raja, *Optik*, **202**, 163714 (2019); https://doi.org/10.1016/j.ijleo.2019.163714
11. A. Ani, P. Poornesh, K.K. Nagaraja, G. Hegde, E. Kolesnikov, I.V. Shchetinin, A. Antony and S.D. Kulkarni, *J. Mater. Sci. Mater. Elem.*, **32**, 22599 (2021); https://doi.org/10.1007/s10854-021-06745-1
12. H.J. Al-Asedy, S.A. Al-khafaji and S.K. Ghoshal, *Opt. Mater.*, **115**, 111028 (2021); https://doi.org/10.1016/j.optmat.2021.111028
13. M. Krasovska, V. Gerbreders, E. Sledevskis, A. Gerbreders, I. Mihailova, E. Tamanisa and A. Ogurcovsa, *Cryst. Eng. Comm.*, **22**, 1346 (2020); https://doi.org/10.1039/C9CE01556F
14. B.K. Sonawane, M.P. Bhole and D.S. Patil, *Physica B*, **405**, 1603 (2010); https://doi.org/10.1016/j.physb.2009.12.050
15. M. Faisal, F.A. Harraz, M. Jalalah, M. Alsaiari S.A. Al-Sayari and M.S. Al-Assiri, *Mater. Today Commun.*, **10**, 1048 (2020); https://doi.org/10.1016/j.mtcomm.2020.101048
16. M. Sathya and K. Pushpanathan, *Appl. Surf. Sci.*, **449**, 346 (2018); https://doi.org/10.1016/j.apsusc.2017.11.127
17. H. Park, W. Son, S.H. Lee, S. Kim, J.J. Lee, W. Cho, H.H. Choi and J.H. Kim, *CrystEngComm*, **17**, 1092 (2015); https://doi.org/10.1039/C4CE02222J
18. S.D. Senol, E. Ozugurlu and L. Arda, *J. Alloys Compd.*, **822**, 153514 (2020); https://doi.org/10.1016/j.jallcom.2019.153514
19. I. Khan, S. Khan, R. Nongjai, H. Ahmed and W. Khan, *Opt. Mater.*, **35**, 1189 (2013); https://doi.org/10.1016/j.optmat.2013.01.019
20. N. Shanmugam, S. Suthakaran, N. Kannadasan and K. Sathish Kumar, *J. Heterocycl.*, **1**, 1 (2015); https://doi.org/10.33805/2639-6734.105
21. S. Sonmezoglu, T. A. Termeli. S. Akin and I. Askeroglu, *J. Sol-Gel Sci. Technol.*, **67**, 97 (2013); https://doi.org/10.1007/s10971-013-3054-1
22. S. Sönmezoðlu and E. Akman, *Appl. Surf. Sci.*, **318**, 319 (2014). https://doi.org/10.1016/j.apsusc.2014.06.187
23. A. Singh, B.P. Nenavathu, Irfan and M. Mohsin, *Chem. Pap.*, **75**, 4317 (2021); https://doi.org/10.1007/s11696-021-01654-3
24. H.L. Porter, J.F. Muth, J. Narayan, J.V. Foreman and H.O. Everitt, *J. Appl. Phys.*, **100**, 123102 (2006); https://doi.org/10.1063/1.2372312
25. L. Umaralikhan and M.J.M. Jaffar, *J. Mater. Sci. Mater. Electron.*, **28**, 7677 (2017); https://doi.org/10.1007/s10854-017-6461-1
26. Z.M. Al-Asady, A.H. Al-Hamdani and M.A. Hussein, *AIP Conf. Proc.*, **2213**, 020061 (2020); https://doi.org/10.1063/5.0000259
27. M. Shkir, M. Anis, S.S. Shaikh, M.S. Hamdy and S. AlFaify. *Appl. Phys. B*, **126**, 121 (2020); https://doi.org/10.1007/s00340-020-07472-x;
28. D.S. Rahman, S.K. Pal, S.S. Singha, S. Kundu, S. Basu and S.K. Ghosh, *Mater. Adv.*, **1**, 2897 (2020); https://doi.org/10.1039/D0MA00362J
29. F. Khosravi-Nejad, M. Teimouri, S.J. Marandi and M. Shariati, *J. Cryst. Growth*, **522**, 214 (2019); https://doi.org/10.1016/j.jcrysgro.2019.06.020